IEICE TRANSACTIONS

on Communications

VOL. E99-B NO. 12
DECEMBER 2016

A PUBLICATION OF THE COMMUNICATIONS SOCIETY
The Institute of Electronics, Information and Communication Engineers
Kikai-Shinko-Kaikan Bldg., 5-8, Shibakoen 3chome, Minato-ku, TOKYO, 105-0011 JAPAN

IEICE TRANS. COMMUN., VOL.E99–B, NO.12 DECEMBER 2016

PAPER

Adaptive Sidelobe Cancellation Technique for Atmospheric Radars Containing Arrays with Nonuniform Gain

Taishi HASHIMOTO[†a)], ***Nonmember***, **Koji NISHIMURA**[††], ***Member***, ***and*** **Toru SATO**[†], ***Fellow***

SUMMARY The design and performance evaluation is presented of a partially adaptive array that suppresses clutter from low elevation angles in atmospheric radar observations. The norm-constrained and directionally constrained minimization of power (NC-DCMP) algorithm has been widely used to suppress clutter in atmospheric radars, because it can limit the signal-to-noise ratio (SNR) loss to a designated amount, which is the most important design factor for atmospheric radars. To suppress clutter from low elevation angles, adding supplemental antennas that have high response to the incoming directions of clutter has been considered to be more efficient than to divide uniformly the high-gain main array. However, the proper handling of the gain differences of main and sub-arrays has not been well studied. We performed numerical simulations to show that using the proper gain weighting, the sub-array configuration has better clutter suppression capability per unit SNR loss than the uniformly divided arrays of the same size. The method developed is also applied to an actual observation dataset from the MU radar at Shigaraki, Japan. The properly gain-weighted NC-DCMP algorithm suppresses the ground clutter sufficiently with an average SNR loss of about 1 dB less than that of the uniform-gain configuration.

key words: *atmospheric radars, partial adaptivity, robust adaptive beamforming, clutter suppression*

1. Introduction

Atmospheric radar observations of mesosphere–stratosphere–troposphere regions generally suffer from clutter at low elevation angles, e.g., ground or sea surface clutter, meteor trail echoes, and aircraft clutter. To suppress this clutter, adaptive beamforming with the output signals from multiple receiver channels has been used in various applications, such as accurate vertical wind velocity measurements [1] and suppressing meteor trail echoes in mesospheric regions [2]. The methodology used in these studies, called robust adaptive beamforming [3], [4], is based on the directionally constrained minimization of power (DCMP) algorithm [5]. This algorithm has an additional constraint regarding the squared norm of the optimal weight, which makes the method robust against error in steering vectors and noise power increases.

The array configurations used in [1], [2] assume that the directional gain function of each receiver channel is uniform. Such a configuration is common in modern atmospheric radars [6]–[8], i.e., a large array is divided into blocks of the same size, and each block has the same number of antennas of the same type. However, clutter is usually present at low elevation angles. In addition, the noise power increase caused by adaptive beamforming is known to heighten as the degree of freedom of the array increases [9]. Therefore, it is considered to be more efficient to add a small number of supplemental antennas that have a high response to low elevation angles, instead of dividing a large array into uniform shapes. Adaptive arrays for such nonuniform-gain configurations are known as partially adaptive antennas [10], [11], and were first applied to atmospheric radar observations by Kamio et al. [12]. Although their developed method (hereafter referred to as the Kamio method) shows that partial adaptivity is effective for atmospheric radars, it requires the gain differences between the main and sub-array to be large enough. Hence, the systems that can use the Kamio method have been limited. In addition, the performance difference between the configurations with uniform and nonuniform gain has not yet been studied.

In this paper, we present the design and evaluation of a partially adaptive beamforming technique for atmospheric radars with proper gain weighting for arrays with nonuniform gain. We first review the gain-weighted norm-constrained (NC)-DCMP algorithm in Sect. 2. The developed method is based on the NC-DCMP algorithm [12], with gain weighting determined by gain differences in the desired direction. We then compare the performances of adaptive beamforming with different configurations, including a six-channel uniform array, and a nonuniform-gain array with the same number of channels. In Sect. 3, these methods are compared in numerical simulations. In Sect. 4, these methods are applied to actual observations by the middle and upper atmosphere (MU) radar at Shigaraki, Japan. Conclusions are presented in Sect. 5.

2. Method

2.1 Basic Methodology

2.1.1 Directionally Constrained Minimization of Power

The DCMP algorithm is an adaptive beamforming method for cases with known desired directions. According to [5], the basic theory of DCMP can be written as a convex optimization problem:

Manuscript received January 29, 2016.
Manuscript revised May 1, 2016.
Manuscript publicized June 21, 2016.

[†]The authors are with Department of Communications and Computer Engineering, Kyoto University, Kyoto-shi, 606-8501 Japan.
[††]The author is with National Institute of Polar Research, Tachikawa-shi, 190-8518 Japan.
a) E-mail: hashimoto.taishi.45z@kyoto-u.jp

DOI: 10.1587/transcom.2016EBP3047

$$\underset{\mathbf{W}}{\text{minimize}}\left(P=\mathbf{W}^{\mathrm{H}}\mathsf{R}_{\mathbf{XX}}\mathbf{W}\right) \text{ subject to } \mathbf{C}^{\mathrm{T}}\mathbf{W}^{*}=H\,, \quad (1)$$

where $(\cdot)^*$ denotes complex conjugation, $(\cdot)^{\mathrm{T}}$ transposition, and $(\cdot)^{\mathrm{H}}$ conjugate transposition of a matrix. Assuming M receivers, $\mathsf{R}_{\mathbf{XX}} \equiv E\left[\mathbf{X}(t)\mathbf{X}^{\mathrm{H}}(t)\right]$ is the covariance matrix of the received signals $\mathbf{X}(t) = [X_1(t), \cdots, X_M(t)]^{\mathrm{T}}$, where $E[\cdot]$ denotes the expectation value. $\mathbf{W}$ is the optimal weight vector, and $\mathbf{C}$ is the directional constraint.

Using the normalized array steering vector $\mathbf{A}(\theta,\phi)$, C_i can be written as

$$C_i = A_i(\theta_o,\phi_o) = \frac{1}{\sqrt{M}}\exp\left(-\frac{2\pi \mathrm{i}}{\lambda}\mathbf{L}_i\cdot\mathbf{V}(\theta_o,\phi_o)\right),$$
$$\mathbf{V}(\theta,\phi) = [\sin\theta\sin\phi, \sin\theta\cos\phi, \cos\theta]^{\mathrm{T}}\,, \quad (2)$$

where λ is the radar wavelength, $\mathbf{L}_i$ $(i = 1,\cdots,M)$ is the geometric location of each receiver, $\mathbf{V}(\theta,\phi)$ is a unit vector in the radial direction (zenith, azimuth) $= (\theta,\phi)$, (θ_o,ϕ_o) is the desired direction, and H is the constraint response. Here, the azimuth angle is measured clockwise from north. The solution to Eq. (1) can be written as follows [5]:

$$\mathbf{W} = \frac{\mathsf{R}_{\mathbf{XX}}^{-1}\mathbf{C}}{\mathbf{C}^{\mathrm{H}}\mathsf{R}_{\mathbf{XX}}^{-1}\mathbf{C}}H^{*}\,. \quad (3)$$

2.1.2 NC-DCMP Algorithm

The NC-DCMP algorithm [3], [4] is a modified DCMP that adds to Eq. (1) the constraint:

$$\|\mathbf{W}\|^2 \le U\,. \quad (4)$$

Here, $\|(\cdot)\|$ denotes the Euclidean norm and U is the norm constraint, which controls the decrease of the signal-to-noise ratio (SNR) caused by the standard DCMP algorithm.

In atmospheric radar applications, U is determined as follows. In the DCMP algorithm, the signal power is assumed to be unchanged when there is no mismatch of the steering vector. Atmospheric radars generally have a very sharp beam; e.g., the half-power full-width of the MU radar is about 3.6° [13]. Backscattering from turbulence is assumed to come only from the volume in this beam; this assumption holds in most cases. In contrast, the noise floor level is proportional to the norm of the optimal weight. The primary noise source in the VHF band is galactic noise, so it is random and independent of antenna gain. Hence, the SNR loss factor L_{SNR} of the DCMP algorithm compared with that of nonadaptive beamforming can be written as follows:

$$L_{\mathrm{SNR}} = 1/\|\mathbf{W}\|^2\,. \quad (5)$$

This equation allows one to limit the SNR loss within L_{dB} dB by setting $U = 10^{-L_{\mathrm{dB}}/10}$.

Generally, the diagonal loading of the covariance matrix is used to solve this problem efficiently [1]:

$$\hat{\mathsf{R}}_{\mathbf{XX}} \equiv \mathsf{R}_{\mathbf{XX}} + \alpha\mathsf{I}\,, \quad (6)$$

where I is an identity matrix and $\alpha > 0$ represents the pseudo-noise added to the covariance matrix. As $\|\mathbf{W}\|^2$ decreases monotonically as α increases, the actual procedure to obtain the optimal weight of the NC-DCMP algorithm is as follows:

1. Set α to a small value.
2. Calculate the optimal weight at α using Eq. (3) and (6). If Eq. (4) holds, then this is the solution.
3. Increase α and repeat steps 2 and 3 until Eq. (4) is satisfied. This can be efficiently performed through any root-finding algorithm such as Newton's method.

Note that the cost function $f(\alpha)$ and its analytical gradient are written as follows:

$$f(\alpha) = \|\mathbf{W}\|^2 - U\,,$$
$$\frac{\partial f(\alpha)}{\partial\alpha} = \frac{\partial\mathbf{W}^{\mathrm{H}}}{\partial\alpha}\mathbf{W} + \mathbf{W}^{\mathrm{H}}\frac{\partial\mathbf{W}}{\partial\alpha}\,, \quad (7)$$
$$\frac{\partial\mathbf{W}}{\partial\alpha} = \left[\mathbf{W}\mathbf{C}^{\mathrm{H}} - \mathsf{I}\right]\hat{\mathsf{R}}_{\mathbf{XX}}^{-1}\mathbf{W}\,.$$

2.2 Kamio Method

Kamio et al. [12] first applied the NC-DCMP algorithm to atmospheric radar with a nonuniform-gain configuration. The system has a high-gain main array supplemented by additional low-gain antennas. In such a system, the weight for the main array is kept at 1, and only the sub-array weights are changed. This constraint prevents the use of the diagonal loading technique, so they used the penalty function method to obtain the solution at high computational cost.

However, we can simplify the solution according to the assumption on which the method is based; i.e., the gain differences between the main and sub-arrays are large enough. Using this assumption, the alternative directional constraint $\bar{\mathbf{C}} = [1,0,0,\cdots]^{\mathrm{T}}$ and constraint response $\bar{H} = 1$ can be adopted in Eq. (1). This enables the diagonal loading approach to be used again, and the method is described as the norm-constrained power inversion algorithm [14] in this case.

If the assumption above fails, however, the norm constraint for the sub-array becomes too large, causing an increase in noise, or cancelling of the desired signal. Therefore, the target radar system is limited to those with large gain differences for the Kamio method.

2.3 Gain-Weighted NC-DCMP Algorithm

Here, we extend the NC-DCMP algorithm to work with any nonuniform-gain array by introducing proper gain weighting into the directional constraint. Suppose there are multiple receiver channels with arbitrary gains in the desired direction (θ_o,ϕ_o); $\mathbf{G}(\theta_o,\phi_o) = [G_1(\theta_o,\phi_o), G_2(\theta_o,\phi_o),\cdots]^{\mathrm{T}}$. By integrating $\mathbf{G}$ into Eq. (1), each element $\hat{C}_i$ $(i = 1,\cdots,M)$ of the modified directional constraint $\hat{\mathbf{C}} = [\hat{C}_1,\hat{C}_2,\cdots]^{\mathrm{T}}$ is defined as follows:

$$\hat{C}_i = C_i\sqrt{G_i(\theta_o,\phi_o)/D}\,, \quad (8)$$

$$D = \frac{1}{M} \sum_{i=1}^{M} G_i(\theta_o, \phi_o)\,.$$

Note $\hat{\mathbf{C}}$ is still appropriately normalized, so Eq. (8) can be used with Eq. (1) without any modification. By strictly handling the gain differences among antennas, the SNR loss remains at the designated value.

The gain of the sub-array antennas in the clutter direction is another important design factor for the algorithm. As the gain weighting reduces the contribution of the sub-array, the clutter suppression capability depends on the gains in the clutter direction. Therefore, the gains between the main and sub-array are preferred to be orthogonal, i.e., the sub-array antennas give no response in the desired direction, and have high gain for low elevation angles. With such gain differences, the method reproduces better the original sub-array NC-DCMP algorithm developed by Kamio et al. [12].

3. Simulation

3.1 System Model

In this simulation, we have two antenna arrays, the "main array" and "sub-array". Figure 1 shows the arrangement of antennas of the radar system. This is based on the MU radar at Shigaraki MU Observatory, Japan [13], [15].

For the main array, 18 groups, which are indicated by the hexagons in Fig. 1, are selected from the center of the MU radar. Each antenna is a three-element crossed Yagi antenna, and the output from all 19 antenna receivers in a group is combined in-phase. The total directional gain of the main array in the azimuth section at $\phi = 0°$ is shown as the solid line (Main) in Fig. 2. The dotted line (Hex) represents the directional gain of a hexagonal subgroup in the main array. The main array is used as a six-channel uniform-gain array or one high-gain array. For the six-channel uniform-gain array, each of the nearest three groups arranged in a regular triangle $3i-2, 3i-1, 3i$ $(i = 1, 2, \cdots, 6)$ are synthesized in-phase. For the high-gain array, the output from all hexagons is uniformly synthesized.

For the sub-array, three different configurations, A, B, and C are considered in this simulation. The directional gain in the azimuth section at $\phi = 0°$ for the channel number 19 of configurations A, B, and C are shown by the dotted, solid, and dashed lines, respectively, in Fig. 3. Type A uses the outer five groups of the MU radar as the sidelobe canceller array, which are indicated as 19–23 in Fig. 1. Each sub-array group consists of 19 antennas, which uses the same antenna as the main array. Type B uses only one antenna from each outer group, indicated by black circles in Fig. 1. Each antenna is the same as that of the main array. Type C also uses the same antenna arrangement as type B, except that each antenna is modeled as a half-wavelength turnstile antenna placed at half wavelength above the ground. Note that type C is considered in this simulation because the ideal element gain function for the sub-array should have an orthogonal response in the beam pattern of the main array, as mentioned in Sect. 2.3. The directional gains of main array and type C antenna are roughly orthogonal, as illustrated in Figs. 2 and 3.

Other radar settings are listed in Table 1. Details about these observation parameters are explained in Sect. 3.2.3.

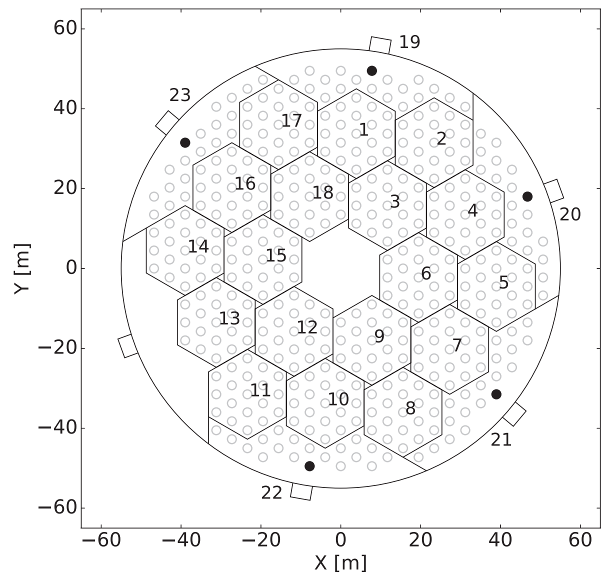

Fig. 1 Antenna position and channel number assignment of the MU radar for both simulation and observation. The five black circles in the outer groups are sub-array antennas used in types B and C.

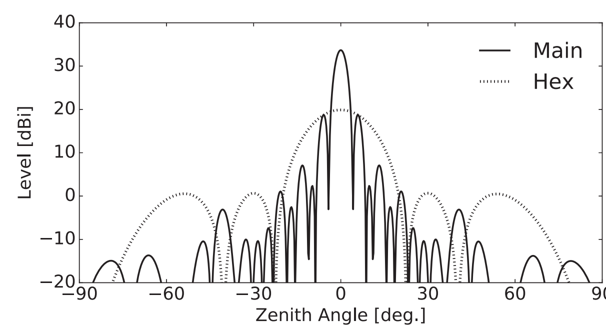

Fig. 2 Azimuth section of one-way directional gains at $\phi = 0°$ for the main array (Main), and one of the main array channel consisting of 19 crossed Yagi antennas indicated by a hexagon in Fig. 1 (Hex).

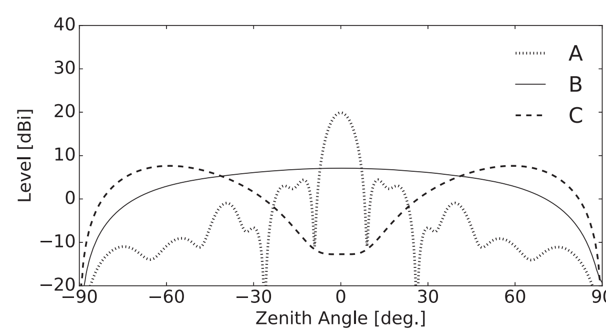

Fig. 3 Azimuth section of one-way directional gains at $\phi = 0°$ for one of the sub-array groups of type A (dotted), B(solid), and C (dashed).

3.2 Signal Generation

In this simulation, there are three kinds of signals: atmospheric echoes, ground clutter, and noise. For the atmospheric echoes, the desired direction (θ_o, ϕ_o) is set to $(0°, 0°)$, and the average peak power of atmospheric echoes P_S is set to 20 dB over the noise floor level $P_N = 1$. The spectral width σ is $1\,\mathrm{m\,s^{-1}}$, and the Doppler shift v_d is set to $1\,\mathrm{m\,s^{-1}}$. For the ground clutter, five point-like sources around the radar are configured. The average power from each source P_I^i $(i = 1, \cdots, 5)$ is 60 dB over the noise floor level P_N. The distance from the radar to each source is 10 km. Directions to each source (θ_i, ϕ_i) are determined by uniform random numbers for each observation: $[60°, 80°]$ for θ_i and $[0°, 360°)$ for ϕ_i. Noise is modeled as complex random numbers that follow the Gaussian distribution with averaged power $P_n = 1$. Further details about signal generation are stated in the following sections.

3.2.1 Atmospheric Echoes

Power spectra of atmospheric echoes can be expressed as a function of the Doppler velocity v, which is assumed to have a Gaussian shape, e.g., in [16]:

$$S(v) = \frac{P_S}{\sqrt{2\pi}\sigma} \exp\left[-\frac{(v - v_d)^2}{2\sigma^2}\right] + P_N\,, \tag{9}$$

where P_S, v_d, σ and P_N are the peak power, Doppler shift, spectral width and noise floor level, respectively, of the spectra of atmospheric echoes. Note that v and the angular Doppler frequency ω have a relationship $v = -\lambda\omega/(4\pi)$, and hence hereafter we replace v in Eq. (9) with this expression. To generate complex time series of atmospheric echoes at each receiver channel $s_i(t)$ $(i = 1, \cdots, M)$, inverse Fourier transform $\mathcal{F}^{-1}[(\cdot)]$ and the steering vector in the desired direction $\mathbf{A}(\theta_o, \phi_o)$ can be used:

$$\begin{aligned} S'(\omega) &= \sqrt{S(\omega)X(\omega)}\angle R(\omega)\,, \\ s_o(t) &= \mathcal{F}^{-1}\left[S'(\omega)\right]\,, \\ s_i(t) &= A_i(\theta_o, \phi_o) g_i(\theta_o, \phi_o) s_o(t)\,, \end{aligned} \tag{10}$$

where $X(\omega)$ and $R(\omega)$ are random numbers that follow the χ^2 distribution with two degrees of freedom and a uniform distribution in $[0, 2\pi)$, respectively. The notation $A\angle B$ means a complex number with amplitude A and argument B. $s_o(t)$ is the generated complex time series at the location $[x, y, z] = [0, 0, 0]$ in the three-dimensional Cartesian coordinates. $A_i(\theta_o, \phi_o)$ and $g_i(\theta_o, \phi_o)$ are the steering vector and directional gain in the desired direction (θ_o, ϕ_o).

3.2.2 Ground Clutter

Ground clutter is modeled as point targets at low elevation angles. The complex time series of the received signal at each receiver channel $u_i(t)$ $(i = 1, \cdots, M)$ from the j-th point target at the direction (θ_j, ϕ_j) can be modeled by

$$u_i^j(t) = \sqrt{P_I^j} A_i(\theta_j, \phi_j) g_i(\theta_j, \phi_j)\,. \tag{11}$$

Here, P_I^j is the power from the j-th clutter signal. Note that Eq. (11) depends only on the incident angle (θ_j, ϕ_j), because each ground clutter signal is modeled as a stationary source and its location is independent of time.

3.2.3 Time Series of Received Signals and Covariance Matrix

Time series of input signals are sampled at discrete intervals for digital signal processing, so we define $k = 1, 2, \cdots$ as the index for sampling time. Input signals $\mathbf{X}(k)$ at sample time k are defined by the sum of signals from all sources:

$$\begin{aligned} \mathbf{X}(k) &= [X_1(k), \cdots, X_M(k)]^{\mathrm{T}}\,, \\ X_i(k) &= s_i(k) + \sum_{j=1}^{5} u_i^j(k) + n_i(k)\,. \end{aligned} \tag{12}$$

The covariance matrix of input signals $\mathsf{R}_{\mathbf{XX}}(k)$ is estimated by the time averaging of $2N_s+1$ snapshots around the current sample time k:

$$\mathsf{R}_{\mathbf{XX}}(k) = \sum_{k_i=k-N_s}^{k+N_s} \mathbf{X}(k_i)\mathbf{X}^{\mathrm{H}}(k_i)\,, \tag{13}$$

where $N_s = 512$ in this simulation.

From Table 1, the interpulse period (IPP) is 400 µs. For every IPP, the observation direction is changed to five different beam directions. In addition, we use 8-bit Spano code [17], and hence 16 consecutive pulses are coherently integrated to take a time sample, making the sampling interval 32 ms. Therefore, $2N_s + 1 = 1025$ snapshots are equivalent to about 32 s.

3.3 Signal Processing

Signals generated by the following four different configurations are processed by the adaptive beamforming methods explained in Sect. 2. The configurations are the six-channel uniform-gain array and the six-channel nonuniform-gain arrays of type A, B, and C. For the uniform-gain configuration, the standard NC-DCMP algorithm is applied. For the

Table 1 Observational parameters of the MU radar.

Center frequency	46.5 MHz
Inter pulse period (IPP)	400 µs
No. of beams	5
Pulse code	8-bit Spano codes
No. of pulse sequence	16
Time resolution	32 ms
Range resolution	150 m
Ranges	1.5 – 25 km
No. of time samples N_t	1024

nonuniform-gain configurations A, B, and C, both the gain-weighted NC-DCMP algorithms and Kamio method [12] are applied; hence seven different configurations in total are compared in this simulation. For the gain-weighted NC-DCMP algorithm, the gain weighting coefficients are determined by the gain differences in the desired direction. The gain difference between the main and a sub-array group is 19 : 1 for type A, 342 : 1 for type B, and 24775.7 : 1 for type C. H is set to 1, and U is set to about 1.12, which is equivalent to limiting the SNR loss to less than 0.5 dB.

Once optimal weights are obtained, the power spectrum density is estimated by the incoherent integration using $N_{\rm I} = 8$ successive periodograms. As shown in Eq. (5), the noise floor increase is proportional to the squared norm of the optimal weight. Because each periodogram uses $N_{\rm v} = N_{\rm t}/N_{\rm I}$ weight vectors, the factor of the noise floor increase $\hat{L}_m$, for the m-th periodogram $S_m(v)$ $(m = 1, \cdots, 8)$, can be estimated as follows:

$$\hat{L}_m = \frac{1}{N_{\rm v}} \sum_{k_m} \|\mathbf{W}(k_m)\|^2 , \tag{14}$$

where $k_m = k + N_{\rm v}(m-1)$ $(k = 1, 2, \cdots, N_{\rm v})$ represents the k-th index in the m-th periodogram. The noise floor increase can be corrected by dividing each periodogram $S_m(v)$ by $\hat{L}_m$:

$$\hat{S}_m(v) = S_m(v)/\hat{L}_m , \tag{15}$$

where $\hat{S}_m(v)$ is the periodogram with SNR loss correction. Finally, the periodogram after the incoherent integration of eight successive periodograms, $\hat{S}(v)$, is written as:

$$\hat{S}(v) = \sum_{m=1}^{8} \hat{S}_m(v) . \tag{16}$$

3.4 Performance Evaluation Method

We generated 100 independent records, and collected the statistical information for all configurations described in the previous section. The clutter suppression ratio (CSR) Z and SNR loss L are first calculated from each periodogram and then converted to the performance index Q by calculating their ratio. The definition of each index is as follows.

Z is defined as the ratio of the decrease of the clutter peak power compared with that obtained by nonadaptive beamforming:

$$Z = 1 - \frac{P_I(\mathbf{W}_{\rm opt})}{P_I^o} , \tag{17}$$

where $P_I(\mathbf{W}_{\rm opt})$ and P_I^o are the clutter power obtained by each signal processing method and nonadaptive beamforming, respectively. Here, $Z = 0$ means no improvement (0%), and $Z = 1$ means that clutter is completely suppressed (100%.)

L is defined as the ratio of the decrease of the peak height of atmospheric echoes in the periodogram normalized by the noise level compared with that obtained by nonadaptive beamforming:

$$L = \frac{P_A^o}{P_A(\mathbf{W}_{\rm opt})} , \tag{18}$$

where $P_A(\mathbf{W}_{\rm opt})$ and P_A^o are the peak power of atmospheric echoes in normalized periodograms obtained by each signal processing method and nonadaptive beamforming, respectively. $L > 1$ represents the SNR loss factor compared with nonadaptive beamforming, and $L = 1$ means there is no change in the noise power.

The performance index Q is defined as:

$$Q = Z/L , \tag{19}$$

which can be interpreted as the clutter suppression capability per unit SNR loss. Note that Q is also in the range from 0 to 1, so we can convert it to a percentage.

3.5 Results and Discussion

Figures 4(a), 4(b), and 4(b) display box-and-whisker plots of the clutter remaining ratio $1 - Z$, SNR loss L, and clutter suppression capability per unit SNR loss Q, obtained for the seven different configurations with over 100 results for each configuration. The configurations are, from left to right, uniform-gain NC-DCMP algorithm, Kamio method with sub-array configurations A, B, and C, and gain-weighted NC-DCMP (GW NC-DCMP) algorithm with A, B, and C. The center line of each box shows the median. The upper and lower edges of the box are the first and third quartiles whereas the whiskers are the upper and lower interquartile ranges.

From Fig. 4(a), the average clutter suppression capabilities are almost perfect for all methods and configurations. Nevertheless, as illustrated in Fig. 4(b), large SNR losses can be observed in the uniform-gain NC-DCMP algorithm and Kamio method with the nonuniform-gain configuration A. Specifically, the average SNR losses are about 0.86 and 1.38 dB for the uniform-gain NC-DCMP algorithm and Kamio method A, respectively. In the uniform-gain configuration, each channel of the main array consists of 19 crossed Yagi antennas with the same element gain functions. In addition, the alignment of the antennas in each group is almost all the same, which makes the reception beam patterns close to each other. Therefore, if there is clutter from a direction where a high sidelobe exists, its suppression is difficult within a designated norm constraint. In contrast, the performance degradation of the Kamio method with the configuration A is attributed to the directionality pattern of the sub-array. As in Fig. 3, the directionality pattern of the each group of type A has lower response to low elevation angles, compared with configurations B or C. This makes it difficult to suppress clutter in low elevation angles within a small norm constraint. In addition, the response in the desired direction of the sub-array is relatively high in this configuration. As we mentioned in Sects. 2.2 and 2.3, the gain differences between the main and sub-arrays must be large for the Kamio method, which is not satisfied in this case.

In contrast, the gain-weighted NC-DCMP algorithm

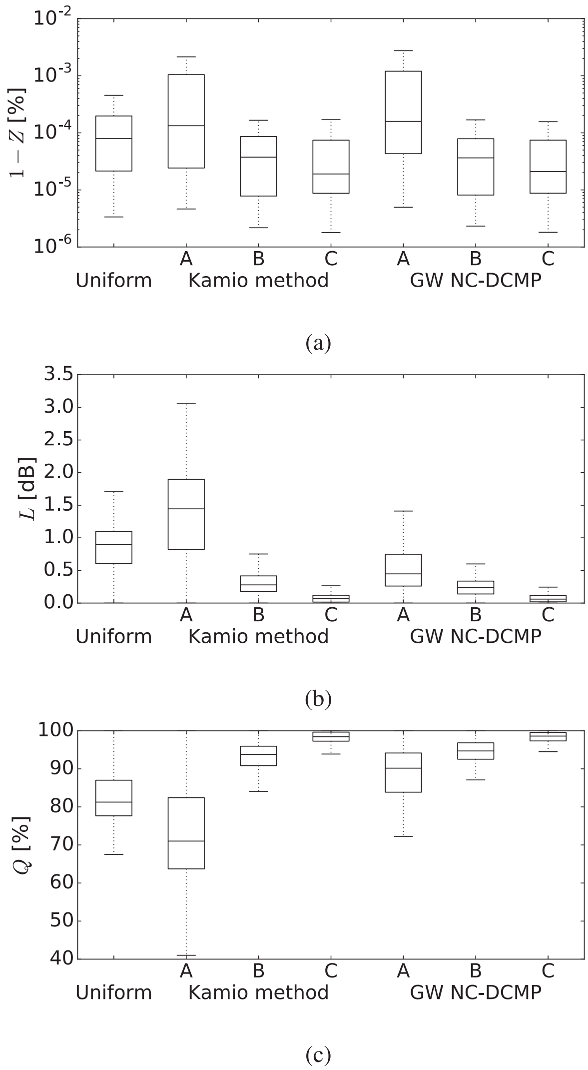

Fig. 4 From top to bottom, (a) clutter remaining ratio $1-Z$, (b) SNR loss L, and (c) clutter suppression ratio per unit SNR loss Q of the seven configurations investigated in the simulation. From left to right, the uniform-gain NC-DCMP algorithm, the Kamio method with the sub-array configurations A, B, and C, and the gain-weighted NC-DCMP algorithm with A, B, and C.

with the configuration A exhibits low SNR losses, at roughly 0.5 dB on average, which is the same order as the permitted SNR loss designated in this simulation. Therefore, the gain-weighted NC-DCMP algorithm can limit the SNR loss as desired with any nonuniform-gain arrays. However, it should be noted that the SNR loss of 0.5 dB is equivalent to a transmitter power loss of 11%, which is roughly proportional to the total cost of the radar system. For atmospheric radars that detect extremely weak scattering echoes, the SNR loss of 0.5 dB is not sufficiently small.

The configuration B is more preferable from this point of view. The average SNR losses are 0.31 and 0.24 dB for the Kamio method and the gain-weighted NC-DCMP algorithm, respectively, as shown in Fig. 4(b). Q results in 93% and 95% for these methods, as shown in Fig. 4(c). The above difference of Q arises from the treatment of the antenna gains of the sub-array. As shown in Figs. 2 and 3, the main array and a sub-array antenna of type B have a gain difference of about 30 dB. However, it is not sufficiently large for the Kamio method in terms of the assumption about the gain difference stated in Sect. 2.2. In contrast, the gain-weighted NC-DCMP algorithm tolerates such a gain difference.

Clearly, configuration C is the best system design, if available, because the sub-array is working as an ideal sidelobe canceller. This configuration has the same $Q = 98\%$ for the Kamio method and gain-weighted NC-DCMP algorithm, as shown in Fig. 4(c). However, not all systems have such ideal gain differences and changing antennas of an existing radar system is usually difficult. Even with non-ideal gain-differences, however, the gain-weighted NC-DCMP algorithm works properly, as seen in configurations A and B.

From the above discussion, we conclude that the gain-weighted NC-DCMP algorithm does sufficiently suppress the clutter at low elevation angles with smaller SNR loss than the uniform-gain NC-DCMP algorithm or the Kamio method. In addition, the gain-weighted NC-DCMP algorithm is shown to have great flexibility in application to any radar systems with non-ideal gain differences. In the next section, these characteristics are confirmed by an actual observation obtained with the same settings as this simulation.

4. Observation

4.1 Observation Settings

An observation was made on July 2, 2015 using the MU radar at Shigaraki, Japan [13], [15]. The MU radar is capable of acquiring the received signal in 25 separate channels [6]. The observation settings are exactly the same as for configuration B in Sect. 3.1. The directional gain of each antenna is shown as B in Fig. 3. Note that these sub-array antennas are chosen from existing parts of the array, so the element gain function cannot be changed as in the simulation in Sect. 3.

As mentioned in Sect. 3.2.3, the duration of each record is about 32 s. We used 110 records taken from 18:00 to 19:00 (LT). The observation has five beam directions, and we used the north beam, i.e., the beam direction (zenith, azimuth) = $(10°, 0°)$.

4.2 Signal Processing

We compared two array configurations: the six-channel uniform-gain array and the six-channel nonuniform-gain array. The uniform-gain NC-DCMP, the sub-array NC-DCMP developed by Kamio et al. [12], and gain-weighted NC-DCMP algorithms are applied to each configuration. Note that signals for each channel are normalized by its noise level before each signal processing method is applied. For this observation, the norm constraint of $U = 1.5$ is used, which is equivalent to a permitted SNR loss of about

1.76 dB. This is the same selection as in [12]. Other parameters are the same as those described in Sect. 3.1.

4.3 Performance Evaluation Method

Similar performance indices to those introduced in Sect. 3.4 can be defined for the observation. The most important difference is that there are ranges where we do not have detectable signals or clutter. To filter these ranges out, the detectability threshold is generally used in atmospheric radars [18], [19]. Detectability is defined as the ratio between the peak height of the signal and the standard deviation of the noise, σ_N, in the spectrum. Also the fluctuation of the noise decreases to $1/\sqrt{N_\mathrm{I}}$ after N_I-time incoherent integration, because the spectra of atmospheric echoes and noise both follow the χ^2 distribution. Therefore, only the ranges with peaks above the following detectability threshold T are considered to have signals:

$$T = \sigma_N \left(1 + D/\sqrt{N_\mathrm{I}}\right), \tag{20}$$

where $D = 3$ is the detectability level.

The CSR, Z, is then calculated by Eq. (17) for the ranges where $P_I(\mathbf{W}_\mathrm{opt}) > T$ and $P_I^o > T$ both hold. The SNR loss, L, can also be defined by Eq. (18) for the ranges where $P_A^o > T$ and $P_A(\mathbf{W}_\mathrm{opt}) > T$. However, the peak positions of the atmospheric echoes need to be estimated, unlike those of the stationary clutter. To do this, we use the periodograms obtained by the uniform-gain NC-DCMP algorithm, because the ground clutter are sufficiently suppressed in this configuration. For each periodogram obtained by the uniform-gain NC-DCMP algorithm, the position of the largest peak is identified. Then, L is calculated by Eq. (18) using the peak power at this position. The clutter suppression capability per unit SNR loss, Q, can be calculated from $Q = Z/L$, as in Eq. (19).

4.4 Results and Discussion

Figure 5(a) is an example of the range profiles of the DC component extracted from the periodogram obtained by the nonadaptive beamforming, uniform-gain NC-DCMP algorithm and gain-weighted NC-DCMP algorithm. The horizontal axis shows the intensity of the ground clutter, and the vertical axis is the range in km. The result of the Kamio method is almost the same as that of the gain-weighted NC-DCMP algorithm, and therefore omitted for brevity. Figure 5(b) is an example of the range section at 5 km. The range is indicated by a horizontal line in Fig. 5(a). The horizontal axis is the Doppler velocity and the vertical axis is the intensity. The bases of the decibel values are the noise level in Figs. 5(a) and 5(b). Figure 6 summarizes the CSR Z, SNR loss L and performance index Q for each signal processing method throughout the observation. The center line of each box shows the median, marks are the means, upper and lower edges of the box are the first and third quartiles, and whiskers are the upper and lower interquartile ranges.

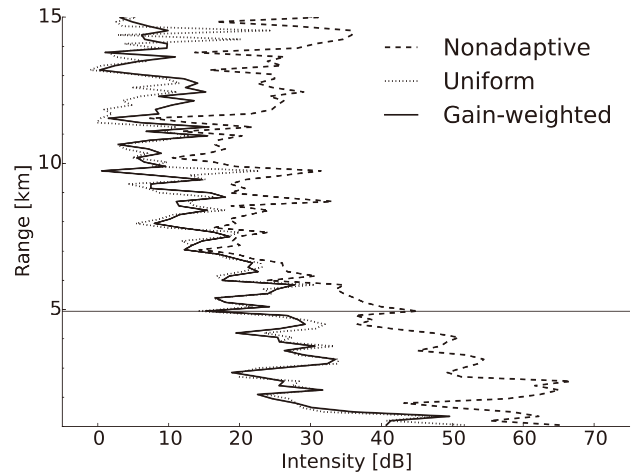

(a)

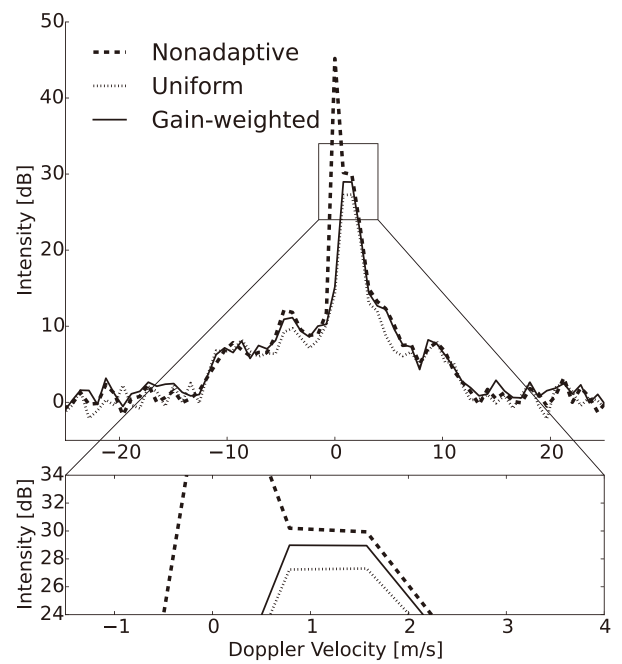

(b)

Fig. 5 (a) Range profile of the DC component, and (b) example of the range section at 5 km, which is indicated by a horizontal line in Fig. 5(a). The dashed line is obtained by nonadaptive beamforming, the dotted line by the six-channel uniform-gain NC-DCMP algorithm, and the solid line by the six-channel gain-weighted NC-DCMP algorithm.

To obtain statistical results, 94 ranges from each record are used, so 10340 periodograms in total are averaged.

As in Fig. 5(a), the gain-weighted NC-DCMP algorithm and uniform-gain NC-DCMP algorithm show similar range profiles of the DC components. In most ranges, both methods sufficiently suppress the ground clutter. Figure 6 also reveals that Z is reasonably similar for all three

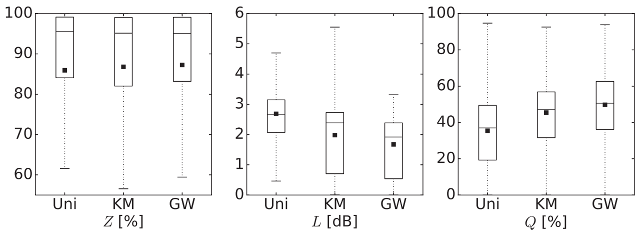

Fig. 6 Comparison of the performance indices Z, L and Q for the uniform NC-DCMP algorithm (Uni), the Kamio method (KM), and the gain-weighted NC-DCMP algorithm (GW) throughout the roughly 1-hour duration of observations.

methods. The gain-weighted NC-DCMP algorithm produces slightly better results than the other two; specifically, Z is 1.3% and 0.5% larger than those of the uniform-gain configuration and the Kamio method, respectively, in average.

In contrast, the peak power of the atmospheric echo obtained by the uniform-gain configuration is about 1 dB lower than that of the gain-weighted NC-DCMP algorithm, as shown in Fig. 5(b). Therefore, the uniform-gain NC-DCMP algorithm gives a higher SNR loss by about 1 dB, equivalently 21% in the linear scale, than the gain-weighted NC-DCMP algorithm, which is a substantial difference in sensitivity.

Also, Fig. 6 shows that the averaged SNR loss L obtained by the gain-weighted NC-DCMP algorithm is 1.7 dB, which is 1.0 and 0.3 dB smaller than the corresponding values of the uniform-gain configuration and Kamio method, respectively. The performance index Q of the gain-weighted NC-DCMP algorithm exhibits in the highest value of 49.7%, which is 14.2% and 4.30% higher than those of the uniform-gain configuration and Kamio method, respectively. These results are consistent with those obtained by the simulation in Sect. 3.

From the discussion above, we can conclude that the gain-weighted NC-DCMP algorithm is the best solution for suppressing the ground clutter in actual observations among the three signal processing methods considered in this paper. The gain-weighted NC-DCMP algorithm can readily suppress the clutter from low elevation angles in actual observations, and the gain weighting limits the SNR loss to a smaller amount than those in other methods. However, as shown in Fig. 4(c), the best element gain function for the sub-array configuration is that with the orthogonal directional gain pattern relative to the main array. Therefore, further observations using such sub-array configurations are required.

5. Conclusion

This paper presented an adaptive sidelobe cancellation technique for atmospheric radars with gain weighting on a nonuniform array. The method introduces gain weighting into the NC-DCMP algorithm in accordance with the gain differences in the desired direction among the receivers.

In Sect. 3, the results of the gain-weighted NC-DCMP algorithm was compared with those of the uniform-gain NC-DCMP algorithm and the Kamio method using numerical simulations. The gain-weighted NC-DCMP algorithm gave sufficient clutter suppression capability with smaller SNR loss than the other two methods, even with non-ideal gain differences between the main array and sub-array. In Sect. 4, the performance of the gain-weighted NC-DCMP algorithm was also tested using actual observations from the MU radar. The gain-weighted NC-DCMP algorithm gave the best clutter suppression capability per unit SNR loss compared with the uniform NC-DCMP algorithm or the Kamio method. In particular, the improvement in the average SNR loss given by the developed algorithm is 1 dB (21%) compared with that of the nonuniform-gain NC-DCMP algorithm, which is substantially different in terms of system sensitivity.

From these results, we conclude that the proper gain weighting is important in suppressing clutter in atmospheric radar signals at low elevation angles. Also, the flexibility of the algorithm, which handles arbitrary gain differences between the main array and sub-arrays, is suitable to extend to any existing atmospheric radar system.

Acknowledgments

Shigaraki MU Observatory is operated by the Research Institute for Sustainable Humanosphere, Kyoto University.

References

[1] K. Nishimura, T. Nakamura, T. Sato, and K. Sato, "Adaptive beamforming technique for accurate vertical wind measurements with multichannel MST radar," J. Atmos. Ocean. Tech., vol.29, no.12, pp.1769–1775, 2012.
[2] T. Hashimoto, K. Nishimura, M. Tsutsumi, and T. Sato, "Meteor trail echo rejection in atmospheric phased array radars using adaptive sidelobe cancellation," J. Atmos. Ocean. Tech., vol.31, no.12, pp.2749–2757, Dec. 2014.
[3] J.E. Hudson, Adaptive Array Principles, IET, 1981.
[4] H. Cox, R. Zeskind, and M. Owen, "Robust adaptive beamforming," IEEE Trans. Acoust., Speech, Signal Process., vol.35, no.10, pp.1365–1376, 1987.
[5] K. Takao, M. Fujita, and T. Nishi, "An adaptive antenna array under directional constraint," IEEE Trans. Antennas Propag., vol.24, no.5, pp.662–669, 1976.
[6] G. Hassenpflug, M. Yamamoto, H. Luce, and S. Fukao, "Description and demonstration of the new middle and upper atmosphere radar imaging system: 1-D, 2-D, and 3-D imaging of troposphere and stratosphere," Radio Sci., vol.43, no.2, 2008.
[7] R. Latteck, W. Singer, M. Rapp, B. Vandepeer, T. Renkwitz, M. Zecha, and G. Stober, "MAARSY: The new MST radar on Andøya-system description and first results," Radio Sci., vol.47, no.1, 2012.
[8] K. Sato, M. Tsutsumi, T. Sato, T. Nakamura, A. Saito, Y. Tomikawa, K. Nishimura, M. Kohma, H. Yamagishi, and T. Yamanouchi, "Program of the antarctic Syowa MST/IS radar (PANSY)," J. Atmos. Sol-Terr. Phys., vol.118, pp.2–15, 2014.
[9] R.T. Compton, "The effect of random steering vector errors in the applebaum adaptive array," IEEE Trans. Aerosp. Electron. Syst., vol.AES-18, no.4, pp.392–400, 1982.
[10] D. Morgan, "Partially adaptive array techniques," IEEE Trans. Antennas Propag., vol.26, no.6, pp.823–833, Nov. 1978.
[11] B. Van Veen and R. Roberts, "Partially adaptive beamformer design

via output power minimization," IEEE Trans. Acoust., Speech, Signal Process., vol.35, no.11, pp.1524–1532, Nov. 1987.
[12] K. Kamio, K. Nishimura, and T. Sato, "Adaptive sidelobe control for clutter rejection of atmospheric radars," Ann. Geophys., vol.22, no.11, pp.4005–4012, 2004.
[13] S. Fukao, T. Sato, T. Tsuda, S. Kato, K. Wakasugi, and T. Makihira, "The MU radar with an active phased array system: 1. Antenna and power amplifiers," Radio Sci., vol.20, no.6, pp.1155–1168, 1985.
[14] R.T. Compton, "The power-inversion adaptive array: Concept and performance," IEEE Trans. Aerosp. Electron. Syst., vol.AES-15, no.6, pp.803–814, 1979.
[15] S. Fukao, T. Tsuda, T. Sato, S. Kato, K. Wakasugi, and T. Makihira, "The MU radar with an active phased array system: 2. In-house equipment," Radio Sci., vol.20, no.6, pp.1169–1176, 1985.
[16] M. Yamamoto, T. Sato, P.T. May, T. Tsuda, S. Fukao, and S. Kato, "Estimation error of spectral parameters of mesosphere-stratosphere-troposphere radars obtained by least squares fitting method and its lower bound," Radio Sci., vol.23, no.6, pp.1013–1021, 1988.
[17] E. Spano and O. Ghebrebrhan, "Pulse coding techniques for ST/MST radar systems: A general approach based on a matrix formulation," IEEE Trans. Geosci. Remote Sens., vol.34, no.2, pp.304–316, March 1996.
[18] K.S. Gage and B.B. Balsley, "Doppler radar probing of the clear atmosphere," Bull. Am. Meteorol. Soc., vol.59, no.9, pp.1074–1093, 1978.
[19] S. Fukao and K. Hamazu, Radar for Meteorological and Atmospheric Observations, Springer Japan, 2014.

Taishi Hashimoto was born in 1986. He received both his B.E. and M.I. degrees from the Department of Informatics, Kyoto University, Japan, in 2010 and 2012, respectively. During the period 2012–2014, he participated in the 54th Japanese Antarctic Research Expedition. He is currently a Ph.D. student at the same university. He is a student member of the American Meteorological Society.

Koji Nishimura received his B.E. degree from Ritsumeikan University, Japan, in 1999, and his M.I. and Ph.D. degrees from Kyoto University, Japan, in 2001 and 2006, respectively. From 2001 to 2003, he worked for Sony Corporation. Since 2007, he has been with the National Institute of Polar Research, Tokyo, Japan, where he is now a project associate professor. His major research interests are radar signal processing, multi-channel signal processing, remote sensing for the atmosphere, and satellite communications. In 2014, Dr. Nishimura received The Prize for Science and Technology (in The Commendation for Science and Technology by the Minister of Education, Culture, Sports, Science and Technology) from the Japanese government. He is a member of the IEEE.

Toru Sato received his B.E., M.E., and Ph.D. degrees in electrical engineering from Kyoto University, Kyoto, Japan in 1976, 1978, and 1982, respectively. He has been with Kyoto University since 1983 and is currently a professor in the Department of Communications and Computer Engineering, Graduate School of Informatics. His major research interests include system design and signal processing aspects of UWB radars, atmospheric radars, radar remote sensing of the atmosphere, and biomedical imaging. He is a fellow of the Institute of Electronics, Information, and Communication Engineers of Japan, and a member of the Society of Geomagnetism and Earth, Planetary and Space Sciences, the Japan Society for Aeronautical and Space Sciences, the Institute of Electrical and Electronics Engineers, and the American Meteorological Society.